Journal of Magnetic Resonance 194 (2008) 29–32

Contents lists available at ScienceDirect

Journal of Magnetic Resonance

journal homepage: www.elsevier.com/locate/jmr

Chemical exchange saturation transfer by intermolecular double-quantum coherence

Wen Ling [a,b], Uzi Eliav [b], Gil Navon [b], Alexej Jerschow [a,*]

[a] Chemistry Department, New York University, New York, NY 10003, USA
[b] School of Chemistry, Tel Aviv University, Ramat Aviv, Tel Aviv 69978, Israel

ARTICLE INFO

Article history:
Received 24 January 2008
Revised 20 May 2008
Available online 4 June 2008

Keywords:
Intermolecular multiple-quantum coherences
Chemical exchange saturation transfer
MRI
Nonlinear dynamics
Distant dipolar field
DDF
iMQC
CEST

ABSTRACT

A number of contrast enhancement effects based on the use of intermolecular multiple-quantum coherences, or distant dipolar field effects are known. This phenomenon is characterized by the dependence on the *m*th power of the initial magnetization (where *m* is the coherence order used). In this paper, we describe the contrast enhancement based on chemical exchange saturation transfer and NOE, which is achieved by the use of intermolecular double-quantum coherences (iDQC). The method was validated using clinically relevant systems based on glycosaminoglycans and a sample of cartilage tissue, showing that the CEST contrast, as well as, NOE are enhanced by iDQC.

1. Introduction

Recently, a large class of chemical exchange saturation transfer (CEST) agents and methods have been introduced to provide a mechanism for contrast enhancement in MRI. Exchangeable groups on molecules, which can be irradiated separately from the water resonance, can transfer their degree of saturation to the large water pool. The changes in the water signal can then be detected with higher sensitivity. Large contrast enhancement factors have been reported [1,2]. The introduction of paramagnetic centers as CEST agents allows one, in principle, to achieve higher enhancement factors if there exists a large induced chemical shift. A related effect is based on the magnetization transfer (MT) effect [3], whereby irradiation off-resonance from the water resonance leads to the saturation of the proton pool on immobilized molecules due to the large homogeneous broadenings arising from dipolar couplings. Examples of applications of the CEST approach include imaging tissue pH [4], mapping brain proteins through their –NH residues [5], monitoring glycogen concentration in the liver [6], mapping specific gene expression in vivo [7], and assessing glycosaminoglycans in tissues [8].

It was recently shown, that the MT effect can be enhanced by combining it with intermolecular multiple-quantum coherences (iMQCs), whereby the contrast effect is raised to the *m*th power (*m* being the coherence order) [9]. In addition, it was shown that the signal modulations in the Goldman–Shen, as well as, in the Edzes–Samulski experiments can be enhanced in a similar manner. The transverse and longitudinal relaxation behaviors of iMQCs have been analyzed [10,11], and the enhancement of *z*-spectrum dips was shown using intermolecular double-quantum coherences (iDQCs) with a simple system of ethanol and water [12].

In this paper, we show that the CEST contrast, as well as, the NOE, can similarly be enhanced by exploiting the iMQC effect in a clinically relevant system. For demonstration purposes, we choose a model system relevant for imaging cartilage, intervertebral discs, heart valves, and the cornea [8], namely solutions of glycosaminoglycans (GAGs), and show a nonlinear enhancement of the contrast due to iDQCs (intermolecular double-quantum coherences). Contrast enhancement is also demonstrated on cartilage tissue, comparing the conventional single quantum (SQ) with the iDQC approach.

2. Theory

The formalism of iMQC was established to describe the formation of multiple echoes and harmonic peaks in NMR experiments [13,14]. Alternatively, one may explain such phenomena using the classical concept of the distant dipolar field, or dipolar

* Corresponding author. Fax: +1 212 260 7905.
E-mail address: alexej.jerschow@nyu.edu (A. Jerschow).

1090-7807/$ - see front matter © 2008 Elsevier Inc. All rights reserved.
doi:10.1016/j.jmr.2008.05.026

demagnetizing field (DDF) [15,16]. While both the classical and the quantum treatments appear equivalent, the quantum description lends itself more readily to the interpretation of experimental results using common NMR concepts such as phase cycling, and coherence selection via pulsed field gradients [13]. By contrast, a quantitative description is typically more easily performed using the classical description. iMQC imaging contrast has also been applied to show structural contrast [17–20] and functional imaging applications have been developed [21].

iMQCs can be created in an experiment simply by applying a hard pulse to a sample at equilibrium. At high temperature, the equilibrium density matrix may be written as

$$\rho_{\mathrm{eq}} = 2^{-N}\prod_i (1 - aI_{zi}), \tag{1}$$

where $a = \frac{\hbar\omega_0}{kT}$. After a hard 90° x-pulse one obtains

$$\rho = 2^{-N}\prod_i (1 + aI_{yi}) = 2^{-N}\left[1 + a\sum_i I_{yi} + a^2\sum_{i,j} I_{yi}I_{yj} + a^3\sum_{i,j,k} I_{yi}I_{yj}I_{yk} + \ldots\right], \tag{2}$$

which contains terms with increasing coherence orders. The different terms can be selected either by phase cycling or by pulsed field gradients.

The application of another pulse leads to the partial creation of intermolecular antiphase coherence. If double-quantum terms are selected between the pulses, the maximum conversion is obtained if the second pulse angle is 60° (for the coherence pathway of $-2 \rightarrow -1$) or 120° (for the coherence pathway of $+2 \rightarrow -1$). This antiphase term then leads to an observable signal via the evolution under intermolecular dipolar couplings [22]. The signal carries a prefactor of a^2 (or $a^{|m|}$ if an m-quantum filtered experiment is performed).

Similarly, the classical theory can be used to derive the signal amplitude as

$$S(t_2) = M_0 i^{-m-1}[mJ_m(\zeta)/\zeta - 1/2\{J_{m-1}(\zeta) - J_{m+1}(\zeta)\}\cos\theta]\exp(-t_2/T_2), \tag{3}$$

where M_0 is the initial magnetization value, J_m the Bessel function of order m, $\zeta = \mu_0\gamma M_0 t_2 \sin\theta$, and θ the flip angle of the second pulse [23]. From this expression one likewise deduces the dependence of the signal on $M_0^{|m|}$, as well as, the dependence on the flip angle, i.e. $(1 + \cos\theta)\sin\theta$ for $m = -2$, and $(1 - \cos\theta)\sin\theta$ for $m = 2$ [23].

Since at the time of the application of the pre-saturation pulse the demagnetizing field is practically zero and the spins contributing to the iDQC signal are expected to be uncorrelated, each of them is affected in the same way as in the conventional CEST experiment. Therefore, it is permissible to write $\langle I_{zi}I_{zj}\rangle = \langle I_{zi}\rangle\langle I_{zj}\rangle$ where $\langle I_{zi}\rangle$ and $\langle I_{zi}\rangle$ denote the expectation values observed in the conventional CEST experiment for the spins that are involved in the iDQC. As a result, the overall M_0^2 dependence of the signal is observed with M_0 representing the magnetization altered from equilibrium by the pre-saturation pulse.

3. Results and discussion

We have recently identified the exchangeable groups on glycosaminoglycans (GAGs), which lend themselves towards measuring GAG concentration via a CEST method in MRI. Every GAG unit has one –NH and several –OH, which can be used as CEST agents.

Fig. 2 shows the results of CEST experiments on samples of varying GAG concentrations. The CEST effect can be quantified by

$$\mathrm{CEST}(\delta) = [S(-\delta) - S(+\delta)]/S(-\delta), \tag{4}$$

where $S(\delta)$ is the signal integral after pre-saturation at the offset δ.

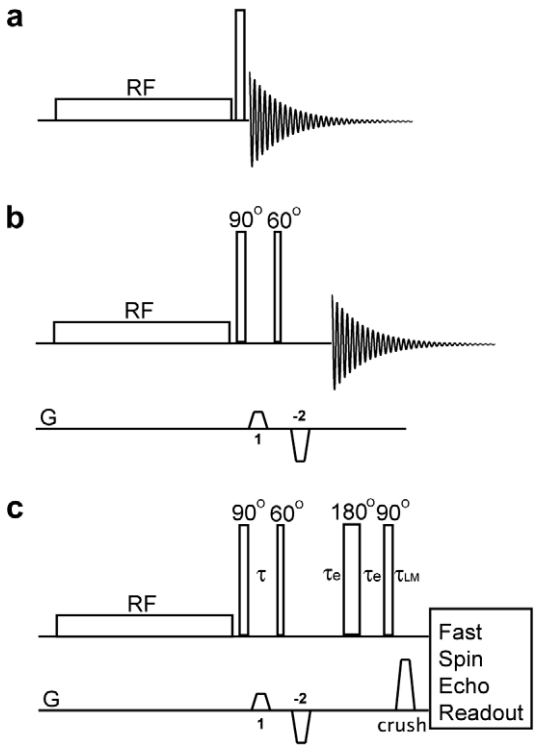

Fig. 1. Pulse sequence for (a) CEST, (b) iDQC CEST, and (c) iDQC CEST imaging.

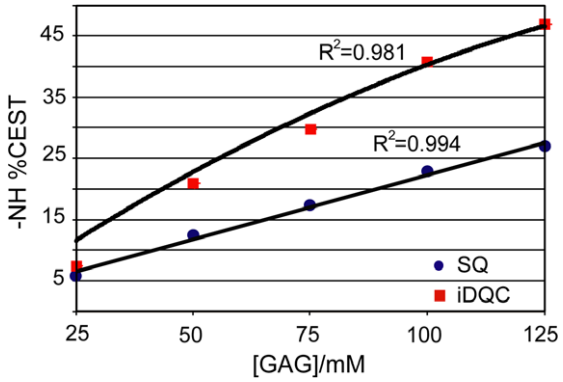

Fig. 2. –NH CEST vs. [GAG] using SQ and iDQC CEST.

The conventional SQ CEST method leads to a linear effect with concentration in the low concentration regime. The CEST effect as measured in the iDQC experiment depends on the square of the initial magnetization M_0, which decreases upon GAG saturation. The iDQC CEST factor can be shown to be

$$\begin{aligned}\mathrm{CEST}_{\mathrm{iDQC}} &= \frac{S_{\mathrm{iDQC}}(-\delta) - S_{\mathrm{iDQC}}(\delta)}{S_{\mathrm{iDQC}}(-\delta)} = \frac{S^2_{\mathrm{SQ}}(-\delta) - S^2{}_{\mathrm{SQ}}(\delta)}{S^2_{\mathrm{SQ}}(-\delta)} \\ &= \frac{S_{\mathrm{SQ}}(-\delta) - S_{\mathrm{SQ}}(\delta)}{S_{\mathrm{SQ}}(-\delta)}\left[2 - \frac{S_{\mathrm{SQ}}(-\delta) - S_{\mathrm{SQ}}(\delta)}{S_{\mathrm{SQ}}(-\delta)}\right] \\ &= 2\mathrm{CEST}_{\mathrm{SQ}} - \mathrm{CEST}^2_{\mathrm{SQ}}\end{aligned} \tag{5}$$

under the weak rf pulse approximation [2]. The result is a second polynomial plot of the form $2p[\mathrm{GAG}]$–$p^2[\mathrm{GAG}]^2$ with p depending on the exchange and relaxation parameters, as well as, on the water content of the sample. At higher concentration this curve will be altered because the CEST effect itself becomes nonlinear.

Fig. 3 shows the comparison between the SQ CEST and the iDQC CEST experiments performed on a cartilage sample. The enhance-

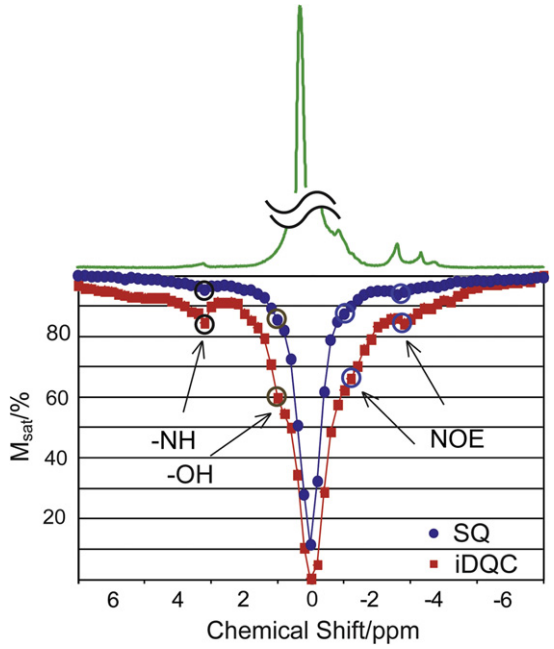

Fig. 3. *z*-spectra using SQ and iDQC CEST on a bovine cartilage specimen.

ment of the CEST effect in the iDQC version is clearly visible for all exchangeable sites, as well as, for the sites that have been identified as NOE-based [8]. Because of the presence of the NOE effect, a conventional MT asymmetry analysis would be misleading for some of the CEST sites due to the overcompensation by NOE in the subtraction step of Eq. (4) as reported in reference [8].

Fig. 4 shows SQ CEST and iDQC CEST images performed on a GAG sample using the hydroxyl protons as the exchangeable groups. The images show $S(\delta = 1\ \text{ppm})/S(\delta = -1\ \text{ppm})$, in which case the SQ and iDQC intensities should compare according to

$$[S(\delta)/S(-\delta)]_{\text{iDQC}} = [S(\delta)/S(-\delta)]^2_{\text{SQ}}. \quad (6)$$

The experimentally observed intensities agree well with this relationship as shown in Fig. 4.

4. Conclusions

We show that contrast based on CEST can be enhanced by combining the experiment with intermolecular double-quantum coherences (iDQCs). This effect is demonstrated with a clinically relevant system (glycosaminoglycan solutions), as well as, on a tissue sample. Two-dimensional images demonstrate directly the squared dependence of the contrast on the initial magnetization. Previously-identified NOE sites are also shown to exhibit this contrast enhancement effect. Using this concept in combination with nonlinear feedback or chaotic spin dynamics [24–27] one may further enhance the contrast of CEST, MT, and NOE imaging, as well as of any other processes that alter the initial magnetization.

5. Experimental

5.1. NMR sample preparation

Five samples with 125, 100, 75, 50, and 25 mM GAG concentrations were prepared from CS A (Aldrich–Sigma, St. Louis, MO, USA) in a standard solution of phosphate buffered saline (PBS, pH = 7.4, cell culture, Aldrich–Sigma). The concentration refers to the number of the disaccharide units in GAG.

The bovine cartilage samples were obtained from a USDA approved slaughter house (Bierig Bros, Vineland, NJ) within 5 h of animal sacrifice (4–6 months old cows) and frozen at −20°C until used. After deicing, the soft tissue was removed first. The samples were cut so as to include every anatomical region of cartilage, and without bone segment, and placed into 5 mm liquid NMR tubes (sample sizes—4 mm in diameter and 5 mm in length). Flourinated oil (Fluorinert, FC-77, Aldrich–Sigma) was filled into the void spaces for reducing susceptibility artifacts.

5.2. NMR hardware

Data are acquired at 11.7 T (500 MHz ^{1}H frequency) using a Bruker Avance spectrometer equipped with a BBO probe. The temperature of the sample was stabilized at 22 °C with a variation of ±0.2 °C.

5.3. NMR experiments

For the single quantum (SQ) CEST experiments, continuous wave irradiation (CW) was used with the irradiation power and duration varying according to the system of interest, followed by a 5° pulse ($\omega_1/2\pi = 6.7$ kHz). The short pulse allows one to reduce the recycle delay and alleviates radiation damping effects. Eight accumulations were used, a spectral window width of 10 kHz and 8192 points were used, and the recycle delay was set to 6 s.

For the iDQC CEST experiments, continuous wave irradiation (CW) was used with the irradiation power and duration varying according to the system of interest, followed by a 90° pulse and a

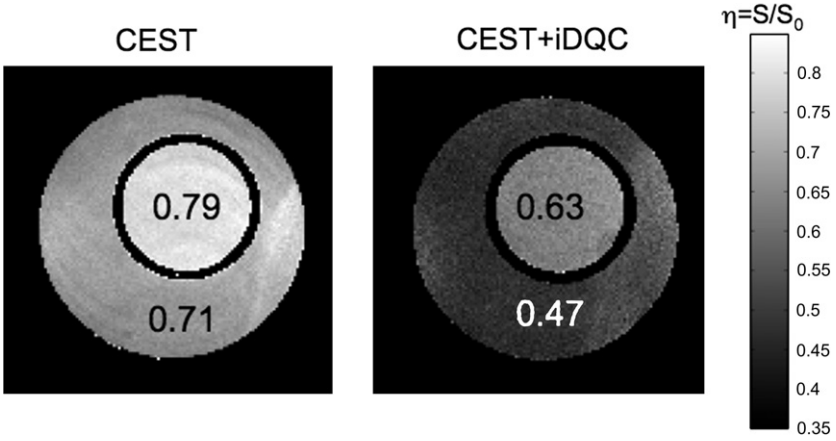

Fig. 4. SQ and iDQC CEST images of a GAG phantom. Inner tube: 44 mM, outer tube: 88 mM GAG.

60° pulse. A combination of phase cycling and pulse field gradients was used to select the intermolecular double-quantum coherence. The phase cycle was $\varphi_{CW} = 0°$, $\varphi_{90°} = k \times 45°$, $\varphi_{60°} = l \times 90°$, and the receiver phase $\varphi_r = k \times 90° - l \times 90°$ with $k = 0,1,2,3,4,5,6,7$ and $l = 0,1,2,3$. Two trapezoid-shaped gradients were used with a duration of 800 μs and 200 μs rise and fall times were applied before and after the 60° pulse, with strengths of 18.4 and −36.8 G/cm, respectively. A spectral window width of 10 kHz, and 8192 points were used, and the recycle delay was set to 10 s.

For measuring the –NH based iDQC/SQ CEST effect, the probe was detuned by +4 MHz to reduce radiation damping effects. The GAG phantoms were irradiated for 6 s at $\delta = \pm 3.2$ ppm, with an irradiation power of 550 Hz ($\delta = +3.2$ ppm is irradiation at the –NH site of GAG, and $\delta = -3.2$ ppm is irradiation on the other side of the water signal). The power level for the other pulses was set to $\omega_1/2\pi = 6.7$ kHz.

For both the SQ and the iDQC z-spectra on cartilage, the probe was tuned on resonance. There was no interference with radiation damping for this sample, mainly due to the much shorter T_2 (typically 20–30 ms in articular cartilage). The CW irradiation power was 50 Hz and the duration 10 s. The power level for the other pulses was set to $\omega_1/2\pi = 23$ kHz. A total of 71 spectra were collected with 100 Hz shift in offset frequency per step. The water intensity was then plotted as a function of the irradiation frequency with respect to the center of the main water resonance.

5.4. Imaging

A Bruker 7.4 T micro-imager was used to obtain the images shown in Fig. 4. The instrument was equipped with a probe of 10 mm diameter and a gradient unit with a rise time of 100 μs and a maximum gradient intensity of 180 G/cm. A sample with two concentric tubes of 5 and 10 mm diameter containing 44 and 88 mM chondriotin sulfate, respectively, was prepared. A saturation power of 85 Hz and duration of 4 s was used in both the conventional CEST experiment as well as the CEST iDQC experiment. The imaging module was a fast spin echo with 4 echoes per scan and TE/TR of 29/7000 ms. The imaging pulse sequence is shown in Fig. 1c. The gradients were of 24.3 and −48.6 G/cm strength and their durations 0.6 ms. Best results were achieved using an echo delay t_e (optimized for the conversion between $T_{2,-1} \rightarrow T_{1,-1}$), followed by a 90° pulse and crusher gradient of 136.1 G/cm strength and 3 ms duration, after which the $T_{1,0}$ component remains. This component is then imaged using a fast spin echo readout. The echo delay t_e was 70 ms and $t_{LM} = 2$ ms. The number of averages was 1 for the SQ CEST measurement and 64 for the combination with iDQC. The image was represented as $S(\delta = +1 \text{ ppm})/S(\delta = -1 \text{ ppm})$.

5.5. Data processing

For both the SQ and iDQC CEST experiments, the integral of water signal was used to plot the CEST effect, the integration region was chosen as ±0.3 ppm with respect to the water signal.

Acknowledgments

The spectroscopy work was supported by the US NSF, Grant CHE-0554400. The imaging and cartilage work was supported by the US NIH, Grant 1R21AR054002-01A1 and by the Israel Science Foundation grant to G.N. A.J. is a member of the New York Structural Biology Center, which is supported by the New York State Office of Science, Technology, and Academic Research and NIH Grant P41 FM66354.

References

[1] K.M. Ward, A.H. Aletras, R.S. Balaban, A new class of contrast agents for MRI based on proton chemical exchange dependent saturation transfer (CEST), J. Magn. Reson. 143 (2000) 79–87.
[2] J. Zhou, P.C.M. van Zijl, Chemical exchange saturation transfer imaging and spectroscopy, Prog. NMR Spectrom. 48 (2006) 109–136.
[3] S.D. Wolff, R.S. Balaban, Magnetization transfer contrast (Mtc) and tissue water proton relaxation invivo, Magn. Reson. Med. 10 (1989) 135–144.
[4] J. Zhou, J.F. Payen, D.A. Wilson, R.J. Traystman, P.C.M. Van Zijl, Using the amide proton signals of intracellular proteins and peptides to detect pH effects in MRI, Nat. Med. 9 (2003) 1085–1090.
[5] J. Zhou, B. Lal, D.A. Wilson, J. Laterra, P.C.M. van Zijl, Amide proton transfer (APT) contrast for imaging of brain tumors, Magn. Reson. Med. 50 (2003) 1120–1126.
[6] P.C.M. van Zijl, C.K. Jones, J. Ren, C.R. Malloy, A.D. Sherry, MRI detection of glycogen in vivo by using chemical exchange saturation transfer imaging (glycoCEST), Proc. Natl. Acad. Sci. USA 104 (2007) 4359–4364.
[7] A.A. Gilad, M.T. McMahon, P. Walczak, P.T. Winnard Jr., V. Raman, H.W.M. van Laarhoven, C.M. Skoglund, J.W.M. Bulte, P.C.M. van Zijl, Artificial reporter gene providing MRI contrast based on proton exchange, Nat. Biotechnol. 25 (2007) 217–219.
[8] W. Ling, R.R. Regatte, G. Navon, A. Jerschow, Assessment of glycosaminoglycan concentration in vivo by chemical exchange saturation transfer: gagCEST, Proc. Natl. Acad. Sci. USA 105 (2008) 2260–2270.
[9] U. Eliav, G. Navon, Enhancement of magnetization transfer effects by intermolecular multiple quantum filtered NMR, J. Magn. Reson. 190 (2008) 149–153.
[10] J.H. Zhong, Z. Chen, S.K. Zheng, S.D. Kennedy, Theoretical and experimental characterization of NMR transverse relaxation process related to intermolecular dipolar interactions, Chem. Phys. Lett. 350 (2001) 260–268.
[11] Z. Chen, Z.W. Chen, J.H. Zhong, Quantitative study of longitudinal relaxation related to intermolecular dipolar interactions in solution NMR, Chem. Phys. Lett. 333 (2001) 126–132.
[12] S.C. Zhang, X.Q. Zhu, Z. Chen, S.H. Cai, J.H. Zhong, Apparent longitudinal relaxation in solutions with intermolecular dipolar interactions and slow chemical exchange, Chem. Phys. Lett. 446 (2007) 223–227.
[13] S. Lee, W. Richter, S. Vathyam, W.S. Warren, Quantum treatment of the effects of dipole–dipole interactions in liquid nuclear magnetic resonance, J. Chem. Phys. 105 (1996) 874–900.
[14] W.S. Warren, W. Richter, A.H. Addreotti, B.T. Farmer, Generation of impossible cross-peaks between bulk water and biomolecules in solution NMR, Science 262 (1993) 2005–2009.
[15] G. Deville, M. Bernier, J.M. Delrieux, NMR multiple echoes observed in solid ^{3}He, Phys. Rev. B 19 (1979) 5666–5688.
[16] R. Bowtell, R.M. Bowley, P. Glover, Multiple spin echoes in liquids in a high magnetic field, J. Magn. Reson. 88 (1990) 641–651.
[17] L.S. Bouchard, W.S. Warren, Multiple-quantum vector field imaging by magnetic resonance, J. Magn. Reson. 177 (2005) 9–21.
[18] L.S. Bouchard, F.W. Wehrli, C.L. Chin, W.S. Warren, Structural anisotropy and internal magnetic fields in trabecular bone: coupling solution and solid dipolar interactions, J. Magn. Reson. 176 (2005) 27–36.
[19] L.S. Bouchard, W.S. Warren, Reconstruction of porous material geometry by stochastic optimization based on bulk NMR measurements of the dipolar field, J. Magn. Reson. 170 (2004) 299–309.
[20] L.S. Bouchard, R.R. Rizi, W.S. Warren, Magnetization structure contrast based on intermolecular multiple-quantum coherences, Magn. Reson. Med. 48 (2002) 973–979.
[21] W. Richter, M. Richter, W.S. Warren, H. Merkle, P. Andersen, G. Adriany, K. Ugurbil, Functional magnetic resonance imaging with intermolecular multiple-quantum coherences, Magn. Reson. Imaging 18 (2000) 489–494.
[22] W.S. Warren, S. Ahn, The boundary between liquidlike and solidlike behavior in magnetic resonance, J. Chem. Phys. 108 (1998) 1313–1325.
[23] Z. Chen, S.K. Zheng, J.H. Zhong, Optimal RF flip angles for multiple spin–echoes and iMQCs of different orders with the CRAZED pulse sequence, Chem. Phys. Lett. 347 (2001) 143–148.
[24] S.Y. Huang, J.D. Walls, Y. Wang, W.S. Warren, Y.Y. Lin, Signal irreproducibility in high-field solution magnetic resonance experiments caused by spin turbulence, J. Chem. Phys. 121 (2004) 6105–6109.
[25] S.Y. Huang, A.P. Chung, Y.Y. Lin, Visualizing feed back-enhanced contrast in magnetic resonance imaging, Concepts Magn. Reson. 30A (2007) 378–393.
[26] S. Datta, S.Y. Huang, Y.Y. Lin, Understanding spin turbulence in solution magnetic resonance through phase space dynamics and instability, Concepts Magn. Reson. 28A (2006) 410–421.
[27] S. Datta, S.Y. Huang, Y.Y. Lin, Contrast enhancement by feedback fields in magnetic resonance imaging, J. Phys. Chem. B 110 (2006) 22071–22078.